J. Fluid Mech. (2014), *vol.* 749, *pp.* 794–817.
doi:10.1017/jfm.2014.241

Fully adaptive turbulence simulations based on Lagrangian spatio-temporally varying wavelet thresholding

Alireza Nejadmalayeri[1], Alexei Vezolainen[1], Giuliano De Stefano[2] and Oleg V. Vasilyev[1,†]

[1]Department of Mechanical Engineering, University of Colorado, Boulder, CO 80309, USA

[2]Dipartimento di Ingegneria Industriale e dell'Informazione, Seconda Università di Napoli, Aversa I-81031, Italy

(Received 1 March 2013; revised 24 April 2014; accepted 25 April 2014)

A new framework for spatio-temporally adaptive turbulence simulations is proposed. The method is based on a variable-fidelity representation that tightly integrates numerics and modelling of subgrid-scale turbulence and aims to capture the flow physics on a near-optimal adaptive mesh. The integration is achieved by combining hierarchical wavelet-based computational modelling with spatially and temporally varying wavelet threshold filtering. The proposed approach provides automatic smooth transition from directly resolving all flow physics to capturing only the energetic/coherent structures, which leads to a dynamically adaptive variable-fidelity approach. The self-regulating continuous switch between different fidelity regimes is accomplished through a two-way feedback mechanism between the modelled dissipation and the local grid resolution, which is based on spatio-temporal variation of the wavelet filtering threshold. The proposed methodology systematically accounts for and exploits the spatial and temporal intermittency of turbulence. Thus, it overcomes the major limitation of all existing wavelet-based multi-resolution techniques, namely, the use of a global thresholding criterion. The procedure consists of tracking the wavelet thresholding factor within a Lagrangian frame by exploiting a Lagrangian path-line diffusive averaging approach, based on either interpolation along characteristics or direct solution of the corresponding evolution equation. This new methodology is tested for linearly forced homogeneous turbulence at different Reynolds numbers and provides very promising results on a benchmark with time-varying prescribed level of turbulence resolution.

Key words: computational methods, turbulence modelling, turbulence simulation

1. Introduction

The growing number of complicated fluid devices and rising challenges of complex turbulent flows across numerous disciplines necessitate the development of robust multi-scale variable-fidelity computational methodologies. A wide range of hybrid

† Email address for correspondence: oleg.vasilyev@colorado.edu

approaches have been attempted in order to smooth the sharp interface between the different existing models, namely, Reynolds-averaged Navier–Stokes (RANS), large eddy simulation (LES), and direct numerical simulation (DNS). However, despite the relatively long history of endeavours, much still remains to be done to match these fundamentally different techniques by constructing a coherent physics-based transition between them. A conceptual problem with most current hybrid approaches is that they are based on the common perception that turbulence modelling and numerical methods are two separate fields of research and, once a turbulence model is developed, any suitable computational approach can be used for its numerical implementation.

Since the first use of wavelets in turbulence (Farge & Rabreau 1988), a very different philosophy of physics-based turbulence modelling has been pursued, namely the direct coupling of numerical methods and physical models within the framework of multi-resolution wavelet analysis. For instance, wavelet-based direct numerical simulation (WDNS) (Fröhlich & Schneider 1996) mainly employs the compression achieved by wavelets; coherent vortex simulation (CVS) (Farge, Schneider & Kevlahan 1999), in addition, decomposes the turbulent field into deterministic (coherent) and stochastic (incoherent) modes; stochastic coherent adaptive large eddy simulation (SCALES) (Goldstein & Vasilyev 2004) resolves the most energetic deterministic (coherent) structures, while modelling the effect of the less energetic coherent/incoherent eddies.

A unique systematic approach that merges the above three different wavelet-based approaches within one single computational framework is introduced in this paper. The proposed methodology makes use of a spatio-temporally varying wavelet thresholding technique that allows for synergistic transition among various levels of user-defined *turbulence resolution/fidelity*, while employing the same governing equations. The approach automatically adjusts the required numerical resolution and model fidelity in space/time adaptive fashion using two-way dynamic coupling between turbulence modelling and adaptive numerical method, which results in a hierarchical adaptive variable-fidelity approach that dynamically tracks the regions of interest in space and time, not only by adapting the numerical grid, but also by adjusting the turbulence model. In the present framework, the transition between WDNS, CVS and SCALES regimes is achieved by continuous adjustment/control of the level of subgrid-scale (SGS) dissipation through spatially and temporally varying wavelet thresholding level: very small thresholds correspond to WDNS, moderately small ones to CVS, and larger values to SCALES. The actual value of the threshold explicitly controls the level of SGS dissipation and, thus, the fidelity of the simulation. The proposed automatic model adaptation stands for a new concept of model refinement, hereafter referred as *m*-refinement. Combined with the grid adaptation mechanism, also known as *h*-refinement, the proposed methodology can be thought as *hm*-refinement. Note that although not explored in this paper, the methodology can be further integrated with the polynomial order refinement, known as *p*-refinement, which could be achieved by locally changing the order of the wavelet transform similarly to the approach suggested by Jameson (1998). This work should be viewed as a proof of concept. The proposed hierarchical variable-fidelity approach is demonstrated in a series of numerical experiments on linearly forced homogeneous turbulence at different Reynolds numbers.

The rest of the paper is organized as follows. After a brief discussion of wavelet thresholding filter (WTF) in § 2, the multi-resolution wavelet-based turbulence modelling hierarchy is introduced and elaborated in § 3. The wavelet-filtered incompressible Navier–Stokes equations are concisely reviewed in § 4, together with

the localized dynamic kinetic-energy-based closure model. The new spatially varying thresholding method is presented in § 5. The results of numerical experiments are presented in § 6. Finally, some concluding remarks are given in § 7.

2. Wavelet thresholding filter

In the wavelet-based approach to the numerical simulation of turbulence the separation between resolved energetic structures and unresolved residual flow is obtained through a nonlinear multi-resolution WTF procedure. The filtering operation is accomplished by applying the wavelet-transform to the unfiltered field, discarding the wavelet coefficients below a given relative threshold ϵ and transforming back to the physical space:

$$\overline{u}_i^{>\epsilon}(\boldsymbol{x}) = \sum_{\boldsymbol{l}\in\mathscr{L}^1} c_{\boldsymbol{l}}^1 \phi_{\boldsymbol{l}}^1(\boldsymbol{x}) + \sum_{j=1}^{+\infty}\sum_{\mu=1}^{2^n-1} \sum_{\substack{\boldsymbol{k}\in\mathscr{K}^{\mu,j} \\ |d_{\boldsymbol{k}}^{\mu,j}|>\epsilon\|u_i\|_{WTF}}} d_{\boldsymbol{k}}^{\mu,j}\psi_{\boldsymbol{k}}^{\mu,j}(\boldsymbol{x}), \tag{2.1}$$

where $\epsilon > 0$ stands for the non-dimensional (relative) threshold parameter, $\|\cdot\|_{WTF}$ being the WTF norm that provides the (absolute) dimensional velocity scale in the ith direction, $\psi_{\boldsymbol{k}}^{\mu,j}$ are wavelets of family μ at level of resolution j, $d_{\boldsymbol{k}}^{\mu,j}$ are the coefficients of the wavelet decomposition, $\phi_{\boldsymbol{l}}^1$ are scaling functions at the coarsest level of resolution, and $c_{\boldsymbol{l}}^1$ are the scaling functions coefficients. In this decomposition, bold subscripts denote an index in n-dimensional space, e.g. $\boldsymbol{k} = (k_1, \ldots, k_n)$, while $\mathscr{L}^1$ and $\mathscr{K}^{\mu,j}$ are n-dimensional index sets associated with scaling functions at the first (coarsest) level of resolution ($\phi_{\boldsymbol{l}}^1$) and wavelets of family μ and level j ($\psi_{\boldsymbol{k}}^{\mu,j}$), respectively. More details on the WTF definition can be found, for instance, in Daubechies (1992), while the type and shape of the wavelets employed in the present work are the ones discussed in Goldstein & Vasilyev (2004).

The application of this wavelet filtering procedure results in the decomposition of the turbulent velocity field into two different parts: a coherent more energetic velocity field $\overline{u}_i^{>\epsilon}$ and a residual less energetic coherent/incoherent one u_i', i.e. $u_i = \overline{u}_i^{>\epsilon} + u_i'$. The key role in the WTF definition (2.1) is played by the non-dimensional relative thresholding level ϵ. This parameter explicitly defines the relative energy level of the turbulent eddies that are filtered out and, consequently, controls the importance of the influence of the residual field on the dynamics of the resolved motions. The major limitation of almost all wavelet-based methods is the use of an *a priori* prescribed wavelet threshold, which is constant in time and uniform in space. The recent development of a time-dependent thresholding strategy has only partially addressed the problem for homogeneous turbulence (De Stefano & Vasilyev 2012). This work explores the use of spatially and temporally varying wavelet thresholding, which tightly follows the space–time evolution of the turbulent flow structures.

3. Multi-resolution wavelet-based turbulence modelling hierarchy

The presence of strong spatial and temporal intermittency and the vast range of flow scales, i.e. from the integral scale down to the Kolmogorov dissipation scale, has promoted the development of multi-resolution approaches to computational modelling of turbulence (Farge & Rabreau 1988). Wavelet-based techniques have been demonstrated to be effective tools to address these challenges mainly because of their temporal/spatial localization of scales, intrinsic adaptiveness of wavelet-based

numerical methods, signal de-noising property, ability to identify and extract coherent/energetic structures, and existence of fast wavelet transform.

The family of wavelet-based turbulence models can be roughly grouped into three main categories: WDNS, CVS, and SCALES. The WDNS method, which was proposed by Fröhlich & Schneider (1996), is an adaptive DNS approach, where the wavelet-based numerical methods are used to solve the wavelet-filtered Navier–Stokes equations with a sufficiently small wavelet threshold to ensure that the ignored motions are insignificant. Due to the compression property of wavelets, the number of DOF (degrees-of-freedom) is reduced compared with DNS using conventional approaches. However, because of the very small threshold values that are required, WDNS is still computationally too expensive and impractical for high-Reynolds-number flow applications. For instance, for two-dimensional decaying turbulence, the spatial computational complexity scales with Reynolds number as $Re^{7/10}$ for WDNS, compared with Re for non-adaptive computations (Kevlahan, Alam & Vasilyev 2007).

The CVS method, which was proposed by Farge *et al.* (1999), is based on the idea that coherent modes are mostly responsible for the evolution of turbulence and the turbulent energy cascade. Thus, a turbulent flow field can be decomposed into an organized *coherent* part and a random *incoherent* part that, for homogeneous turbulence, has been shown to represent Gaussian white noise (Farge & Schneider 2001). The coherent structures (corresponding to the wavelet de-noised vorticity field) are simulated directly, while the effect of the incoherent structures is neglected since they provide no turbulent dissipation. CVS achieves a significant compression compared with WDNS. However, the number of retained active modes remains large and the process of calculating the optimal threshold for de-noising at each time-step is quite expensive, since it requires the variance of the incoherent modes. Moreover, the wavelet-based coherent vortex extraction for inhomogeneous turbulence is still an open question (Schneider & Vasilyev 2010).

The SCALES approach, which was proposed by Goldstein & Vasilyev (2004), is a wavelet-based methodology for numerical simulations of turbulent flows that resolves energy-containing motions using wavelet multi-resolution decomposition and self-adaptivity. In the original formulation of the method, the extraction of the most energetic structures is achieved using the WTF procedure with an *a priori* prescribed threshold. The SCALES approach inherits the advantages of both CVS and LES, while overcoming the shortcomings of both methods. Unlike coherent/incoherent and large/small structures decomposition in CVS and LES, respectively, in SCALES the separation is between more and less energetic structures. Also, differently from CVS, the effect of the flow structures that are filtered out cannot be ignored but, similarly to conventional non-adaptive LES, needs to be modelled. Furthermore, the filtering process and, consequently, the SGS modelling procedure benefit from the wavelet nonlinear multi-scale band-pass filter, which depends on the instantaneous flow realizations. The use of SGS models results in the further reduction of the number of DOF compared to CVS and, thus, a higher grid compression is achieved.

The overall at-a-glance comparison of the wavelet-based turbulence modelling techniques (WDNS, CVS and SCALES) and the conventional non-wavelet-based methods (DNS and LES) can be clearly illustrated by means of the coherency diagram reported in figure 1 (Goldstein & Vasilyev 2004). The diagram illustrates the role of coherent structures in the interaction of resolved and residual velocity fields and SGS modelling. The horizontal axis represents the resolved wavenumbers, while the vertical axis corresponds to the wavelet threshold. By inspection of the

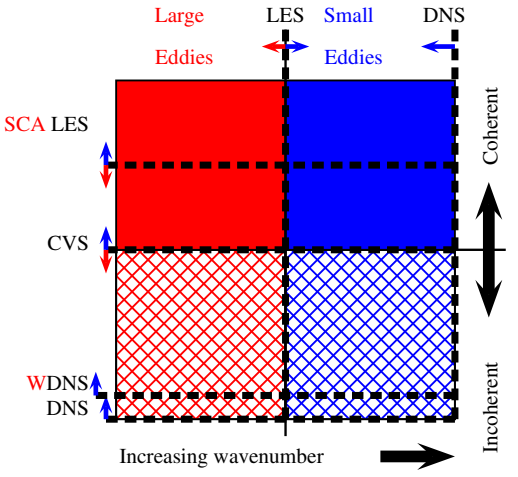

FIGURE 1. (Colour online) Coherency diagram: at-a-glance comparison of wavelet-based approaches (WDNS, CVS and SCALES) with conventional non-adaptive methods (DNS and LES) (Goldstein & Vasilyev 2004).

diagram, CVS and LES can be seen as the limiting cases of coherent/incoherent and large/small structure distinctions, respectively. In the SCALES approach, both resolved and unresolved eddies are not limited to the above formal separations: the majority of energetic structures are resolved, while the effect of both coherent-deterministic and incoherent-stochastic unresolved modes is modelled. Therefore, differently from CVS, the SCALES method is not in practice limited to homogeneous turbulence. On the other hand, differently from LES, the distinction between resolved and unresolved motions is not limited to the size of the structures, which is rather less informative, but depends on the energetic content of the turbulent motions. In addition, the resolved structures and the modelled residual eddies share a range of wavenumbers, thus allowing the turbulent energy cascade to be more realistically captured.

In order to consistently switch from one computational approach to another, it is essential that the different methods share the same structure of governing equations. CVS in its original formulation (Farge *et al.* 1999) solves the wavelet-filtered vorticity equations, with the use of orthogonal Daubechies wavelets (Daubechies 1992), while SCALES solves wavelet-filtered Navier–Stokes equations, supplied with an SGS model, using bi-orthogonal second-generation interpolated wavelets (Sweldens 1996). However, Goldstein & Vasilyev (2004) showed that the turbulent velocity field can be directly decomposed into deterministic coherent and stochastic incoherent (with Gaussian probability density function) modes by applying the WTF operation (2.1) with sufficiently low values of ϵ. Therefore, incompressible CVS can also be based on a velocity–pressure formulation. This way, both CVS and SCALES solve the wavelet-filtered Navier–Stokes equations, without and with the aid of SGS models, respectively, though at different thresholding levels. Finally, WDNS can be also viewed as the solution of the same no-modelled equations with an even smaller value of the threshold parameter.

The fidelity for wavelet-based methods is controlled by the value of the thresholding factor. Very small thresholds correspond to WDNS, moderately small ones to CVS, larger values along with the use of SGS models result in SCALES and much larger thresholds lead to the wavelet-based unsteady RANS (WURANS) approach (Liu &

Vasilyev 2006). The careful combination of the present hybrid WDNS/CVS/SCALES approach with WURANS, in a systematic manner, provides a fully adaptive wavelet-based hybrid method with model form adaptation. However, in addition to changing/controlling the wavelet thresholding factor, the complete method requires the development of new model coupling strategies specific to wavelet methods, similar to those adopted by other hybrid methods (Chaouat & Schiestel 2005; Schiestel & Dejoan 2005; Girimaji & Wallin 2013). This work is currently underway.

In the present framework, the back and forth transition between WDNS and CVS is straightforward. Since neither approaches utilizes any SGS model, the only difference is in the different level of thresholding. On the contrary, the transition from CVS to SCALES (and vice versa) is apparently more difficult. An additional effort for switching on (and off) the SGS modelling procedure, by monitoring/controlling the numerical dissipation induced by the WTF truncation, would be required. More practically, the modelled wavelet-filtered governing equations can be resolved in both CVS and SCALES regimes, while continuously adjusting the level of SGS dissipation through spatially and temporally varying thresholding level. The actual value of the threshold explicitly controls the level of SGS dissipation and, thus, the fidelity of the simulation.

In the current computational framework, the different methods in the wavelet-based turbulence modelling hierarchy (WDNS, CVS, and SCALES) make use of the parallel adaptive wavelet collocation method (PAWCM) (Nejadmalayeri 2012), a dynamically adaptive multi-resolution variable-order approach based on second-generation bi-orthogonal wavelets (Sweldens 1996).

4. Wavelet-filtered Navier–Stokes equations

The SCALES equations, which govern the evolution of coherent energetic structures, are obtained by filtering the incompressible Navier–Stokes equations using the WTF procedure (2.1). For linearly forced isotropic turbulence, the following filtered equations are considered (De Stefano & Vasilyev 2010):

$$\partial_{x_i} \overline{u}_i^{>\epsilon} = 0, \tag{4.1}$$

$$\partial_t \overline{u}_i^{>\epsilon} + \partial_{x_j} \left(\overline{u}_i^{>\epsilon} \overline{u}_j^{>\epsilon} \right) = -\partial_{x_i} \overline{P}^{>\epsilon} + \nu \partial^2_{x_j x_j} \overline{u}_i^{>\epsilon} - \partial_{x_j} \tau^*_{ij} + Q \overline{u}_i^{>\epsilon}, \tag{4.2}$$

where ν is kinematic viscosity, $\tau^*_{ij} = \tau_{ij} - (1/3)\tau_{kk}\delta_{ij}$ stands for the deviatoric part of the unresolved SGS stresses tensor $\tau_{ij} = \overline{u_i u_j}^{>\epsilon} - \overline{u}_i^{>\epsilon}\, \overline{u}_j^{>\epsilon}$, which needs to be modelled. The last term on the right-hand side of (4.2), $Q\overline{u}_i^{>\epsilon}$, represents the linear forcing term (Lundgren 2003; Rosales & Meneveau 2005), which is applied in the physical space over the whole range of wavenumbers (De Stefano & Vasilyev 2010).

In the above governing equations, the notation $\overline{(\cdot)}^{>\epsilon}$ denotes wavelet-filtered quantities. However, the bar symbol for the pressure variable, $\overline{P}^{>\epsilon} = \overline{p}^{>\epsilon}/\rho + (1/3)\tau_{kk}$, does not imply the application of the WTF operator, but is used for consistency with the other terms. The pressure term in the filtered momentum equation must be viewed as a Lagrange multiplier enforcing the incompressibility constraint, since the present WTF is not based on a divergence-free wavelet basis. The present governing equations are similar to the LES ones with the exception that the nonlinear multi-scale band-pass wavelet filter, which depends on the instantaneous flow realization, is used. In this context, the SGS stresses represent the effect of unresolved less energetic deterministic coherent and stochastic incoherent eddies on the resolved energetic coherent structures.

In this study, the SCALES governing equations are closed using the localized kinetic-energy-based model proposed in De Stefano, Vasilyev & Goldstein (2008). This modelling procedure involves the numerical solution of an additional evolution equation for the SGS kinetic energy k_{sgs}, which implicitly takes into account the local energy transfer between resolved and unresolved scales. The model is based on the classical eddy-viscosity concept, where the turbulent viscosity depends on the SGS kinetic energy, differently from the Smagorinsky model in which it depends on the resolved rate of strain. Namely, by assuming the eddy viscosity $\nu_t = C_\nu \Delta k_{\rm sgs}^{1/2}$, the deviatoric part of the unknown SGS stresses tensor is approximated as

$$\tau_{ij}^* \cong -2C_\nu \Delta k_{sgs}^{1/2} \overline{S}_{ij}^{>\epsilon}, \tag{4.3}$$

where Δ is the local wavelet-filter characteristic width. The SGS dissipation, i.e. the rate of local transfer of energy from energetic resolved eddies to unresolved structures, is obtained by definition as $\Pi = -\tau_{ij}^* \overline{S}_{ij}^{>\epsilon}$. Hence, by replacing the above approximate expression for the deviatoric part of SGS stresses, the SGS dissipation rate is approximated in terms of the SGS kinetic energy as

$$\Pi \cong C_\nu \Delta k_{sgs}^{1/2} |\overline{S}_{ij}^{>\epsilon}|^2, \tag{4.4}$$

where $\overline{S}_{ij}^{>\epsilon} = (1/2)\left(\partial_{x_j} \overline{u}_i^{>\epsilon} + \partial_{x_i} \overline{u}_j^{>\epsilon}\right)$ is the resolved rate-of-strain tensor and $|\overline{S}_{ij}^{>\epsilon}| = \left(2\overline{S}_{ij}^{>\epsilon} \overline{S}_{ij}^{>\epsilon}\right)^{1/2}$ stands for its modulus.

The model transport equation for the SGS kinetic energy is expressed as follows (Ghosal *et al.* 1995):

$$\partial_t k_{sgs} + \overline{u}_j^{>\epsilon} \partial_{x_j} k_{sgs} = \partial_{x_j}[(\nu + \nu_t)\partial_{x_j} k_{sgs}] - \tilde{\varepsilon}_{sgs} + \Pi, \tag{4.5}$$

where $k_{sgs}(\boldsymbol{x}, t)$ is defined as the difference between the wavelet-filtered kinetic energy $\overline{k}^{>\epsilon}$ and the kinetic energy of the resolved velocity field k_{res}

$$k_{sgs} = \overline{k}^{>\epsilon} - k_{res} = \tfrac{1}{2}\left(\overline{u_i u_i}^{>\epsilon} - \overline{u}_i^{>\epsilon} \overline{u}_i^{>\epsilon}\right). \tag{4.6}$$

The SGS viscous dissipation $\tilde{\varepsilon}_{sgs}$ on the right-hand side of (4.5) is analogously defined as the difference between the wavelet-filtered pseudo-dissipation $\overline{\tilde{\varepsilon}}^{>\epsilon}$ and the pseudo-dissipation of the resolved velocity field $\tilde{\varepsilon}_{res}$,

$$\tilde{\varepsilon}_{sgs} = \overline{\tilde{\varepsilon}}^{>\epsilon} - \tilde{\varepsilon}_{res} = \nu\left(\overline{\partial_{x_j} u_i \partial_{x_j} u_i}^{>\epsilon} - \partial_{x_j} \overline{u}_i^{>\epsilon} \partial_{x_j} \overline{u}_i^{>\epsilon}\right). \tag{4.7}$$

Similarly to the SGS stress model (4.3), the SGS viscous dissipation can be modelled using simple scaling arguments as

$$\tilde{\varepsilon}_{sgs} = C_\varepsilon \Delta^{-1} k_{sgs}^{3/2}. \tag{4.8}$$

Therefore, the present SGS modelling procedure results in two dimensionless model parameters: *turbulent eddy-viscosity* model coefficient C_ν and *SGS energy dissipation* model coefficient C_ε. Both model parameters C_ν and C_ε could be determined as pointwise functions of space and time by exploiting classical dynamic procedures, using either a Bardine-like or a Germano-like approach (De Stefano & Vasilyev 2010). In this work, for the sake of simplicity and in order to save computational resources, the LKM procedure is used, where the model parameters are assumed to be *a priori* prescribed as $C_\nu = 0.06$ and $C_\varepsilon = 1.0$ (De Stefano *et al.* 2008).

5. Spatially varying thresholding for adaptive fidelity simulations

Until now, almost all wavelet-based turbulence modelling approaches, as well as all wavelet-based methods for numerical solution of partial differential equations, have employed an *a priori* defined thresholding parameter ϵ for the WTF definition (2.1). The main objective of this work is to enhance the robustness of the wavelet approach, by exploring the physics-based spatially and temporally variable thresholding strategy. The proposed spatio-temporally varying thresholding methodology is the key element of a more general wavelet-based hybrid turbulence modelling framework, which fully utilizes spatial/temporal turbulent flow intermittency.

Previous studies have demonstrated that in SCALES the SGS dissipation increases with the WTF level, being proportional to ϵ^2 (Goldstein, Vasilyev & Kevlahan 2005). This implies that the rate of local energy transfer from energetic resolved eddies to unresolved less energetic structures (and vice versa) can be controlled by varying the thresholding factor. In fact, a decrease of the thresholding level ϵ results in the local grid refinement with the subsequent rise of the resolved viscous dissipation, while an increase of ϵ leads to mesh coarsening that results in the growth of the local SGS dissipation. Therefore, the SCALES methodology can be improved by exploiting a spatially varying threshold as a way to control the SGS dissipation. The basic idea is to locally vary ϵ wherever the level of modelled dissipation (4.4) deviates from an *a priori* defined magnitude.

In order to vary ϵ in a physically consistent fashion, it should follow the local flow structures as they evolve in space and time, thus necessitating the Lagrangian representation of the WTF parameter. Differentiation with respect to time of the statistical average of ϵ along the trajectory of a fluid particle results in the evolution equation for ϵ based on the material derivative. The adjustment of the wavelet threshold $\epsilon(\boldsymbol{x}, t)$ is achieved within the material framework through spatially and temporally varying forcing. Since the chaotic convective mixing can create high-frequency modes in the threshold field and consequently lead to undesired small-scale fluctuations in the velocity field, an additional artificial diffusion term is added to the evolution equation. This way, the Lagrangian representation of ϵ can be achieved by solving the following evolution equation based upon the Lagrangian path-line diffusive averaging approach (Vasilyev *et al.* 2008):

$$\partial_t \epsilon + \overline{u}_j^{>\epsilon} \partial_{x_j} \epsilon = -\text{forcing}_\epsilon(\boldsymbol{x}, t) + \nu_\epsilon \partial^2_{x_j x_j} \epsilon. \tag{5.1}$$

To avoid the creation of undesired small scales, the numerical diffusion time scale, Δ^2/ν_ϵ, should be comparable with the convective time scale associated with the local rate of strain, i.e. $|\overline{S}_{ij}^{>\epsilon}|^{-1}$, which results in the Smagorinsky-like viscosity coefficient $\nu_\epsilon(\boldsymbol{x}, t) = C_{\nu_\epsilon} \Delta^2 |\overline{S}_{ij}^{>\epsilon}|$, where C_{ν_ϵ} is a dimensionless coefficient of the order unity. That guarantees the smoothness of the spatially varying threshold.

For the sake of efficiency, instead of directly solving (5.1), the evolution of ϵ can be also obtained by considering the linear (or higher-order) interpolation along characteristics, similarly to what was proposed by Meneveau, Lund & Cabot (1996):

$$\frac{1}{\Delta t}\left[\epsilon^{new}(\boldsymbol{x}, t + \Delta t) - \epsilon^{old}(\boldsymbol{x} - \overline{\boldsymbol{u}}^{>\epsilon} \Delta t, t)\right] = -\text{forcing}_\epsilon(\boldsymbol{x} - \overline{\boldsymbol{u}}^{>\epsilon} \Delta t, t). \tag{5.2}$$

In fact, the use of linear interpolation results in sufficient numerical diffusion, thus eliminating the need for explicit additional diffusion. Finally, the required diffusion is controlled either explicitly, by directly solving the evolution equation (5.1), or implicitly, through the local interpolation procedure used in (5.2).

The proposed spatio-temporally varying thresholding strategy ensures that the wavelet threshold is determined 'on the fly' according to the desired level of *turbulence resolution*. The latter is measured by the local fraction of SGS dissipation (FSGSD) that is defined as

$$\mathcal{F}(\boldsymbol{x}, t) = \frac{\Pi}{\varepsilon_{res} + \Pi}, \tag{5.3}$$

where $\varepsilon_{res} = 2\nu \overline{S}_{ij}^{>\epsilon} \overline{S}_{ij}^{>\epsilon}$ is the resolved viscous dissipation. A prescribed level for the quantity $\mathcal{F}$ determines the level at which the most energetic structures are resolved and the effect of SGS residual motions is modelled.

Thus, the forcing mechanism for the WTF level evolution, according to either (5.1) or (5.2), is based on the FSGSD variable (5.3), which is utilized as controlling parameter. It is worth noting that the SGS kinetic energy increases with the threshold level. Consequently, the ratio $k_{sgs}/(k_{res} + k_{sgs})$ could be alternatively used to characterize how much the turbulent flow is resolved/modelled. However, since the energy spectrum decreases with wavenumber, the SGS kinetic-energy-based characterization of turbulence resolution is not appropriate for high-Reynolds-number flows. In fact, being mostly based on large-scale contributions, this measure would not be adequately sensitive to the increase of wavenumber range with the Reynolds number. On the other hand, the SGS dissipation-based characterization represents a more objective measure, since the peak of the dissipation spectrum increases with wavenumber. Furthermore, depending on the closure model that is employed, the SGS kinetic energy variable is not always available, while modelled and resolved dissipations are. For these reasons, in this work the thresholding parameter ϵ is adapted based on the ratio of dissipations, rather than the ratio of kinetic energies, of modelled and resolved structures.

Based on this concept of turbulence resolution, the forcing scheme is basically designed to maintain the FSGSD variable $\mathcal{F}$ at the *a priori* defined *goal* value $\mathcal{G}$. The forcing term on the right-hand side of (5.1) (or, equivalently, (5.2)) ensures that $\mathcal{F}$ is directly controlled, in conjunction with the use of a relaxation time parameter τ_ϵ. In this study the following simple linear feedback forcing scheme is assumed:

$$\text{forcing}_\epsilon\,(\boldsymbol{x}, t) = \frac{H(\Pi)}{\tau_\epsilon} \left(\frac{\Pi}{\varepsilon_{res} + \Pi} - \mathcal{G} \right) \epsilon. \tag{5.4}$$

It is important to emphasize that the definition (5.4) is general enough to be used together with SGS models that allow for local energy backscatter. The generality is achieved by using the Heaviside function $H(\cdot)$, which turns the forcing off in regions of negative SGS dissipation. In practice, where energy backscatter occurs, the threshold is not modified and the inverse cascade of energy is captured by adjusting the computational mesh, without altering the relative energy level of the resolved structures.

As far as the relaxation time coefficient τ_ϵ is concerned, following the time-varying threshold study of De Stefano & Vasilyev (2012), a time scale associated with the characteristic rate of strain is chosen. The same volume-averaged relaxation time scale $\tau_\epsilon^{-1} = \langle |\overline{S}_{ij}^{>\epsilon}| \rangle$ has been successfully tested for the present space–time-varying methodology with linear interpolation (5.2) in Nejadmalayeri *et al.* (2011). Numerical simulations of linearly forced homogeneous turbulence, where the turbulent resolution is maintained at different prescribed goal values for many eddy turnover times,

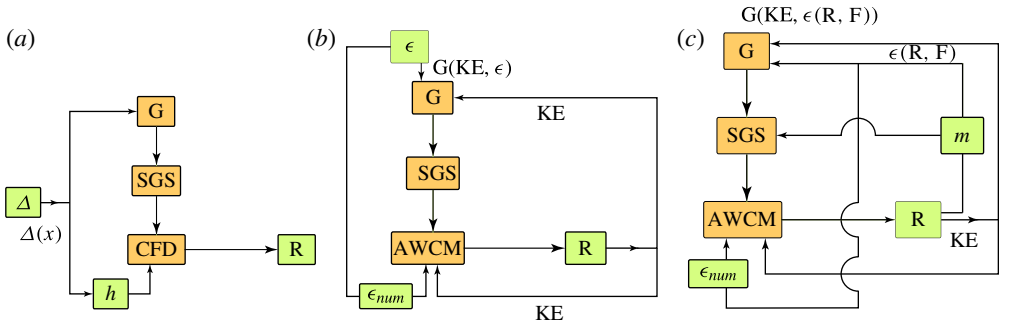

FIGURE 2. (Colour online) Dependency diagram for (*a*) classical explicitly filtered LES, (*b*) original SCALES with prescribed thresholding level, and (*c*) new variable-fidelity *m*-SCALES. Notation: G, filter; R, results; *m*, model refinement; Δ, prescribed LES filter width; ϵ, wavelet threshold for model adaptation; ϵ_{num}, wavelet threshold controlling the accuracy of the solution; F, arbitrary dynamically important physical quantity to be controlled: *h*, grid spacing.

have been conducted. In this study, to fully exploit the local intermittency of the turbulent eddies, instead of a global coefficient, the corresponding local time scale, $\tau_\epsilon^{-1}(\boldsymbol{x}, t) = |\overline{S}_{ij}^{>\epsilon}|$, is used.

To summarize, the present Lagrangian variable thresholding is a new strategy for the SCALES method that provides a two-way feedback mechanism between the modelled dissipation and the computational mesh. This allows an *a priori* defined level of SGS dissipation to be maintained, namely, a prescribed degree of turbulence resolution for the ongoing simulation. The feedback is achieved through spatio-temporal variation of the wavelet threshold that follows the evolution of the resolved flow structures. The proposed methodology represents a *fully adaptive WTF*-based approach to turbulent flow simulation.

In order to highlight the differences, the variable-fidelity SCALES method, for brevity hereafter referred to as *m*-SCALES, is compared to the original SCALES approach with constant thresholding, as well as to the classical explicitly filtered LES method. The general connections of the solver components are reported for each case in the dependency diagram shown in figure 2. It is apparent how *m*-SCALES connects all components integrating numerics/model/physics together, which leads to a fully dynamically adaptive computational framework.

In the classical non-adaptive explicitly filtered LES, the filter width is fixed *a priori*, resulting in the implicit definition of the grid resolution. Therefore, both the CFD solver (through the mesh spacing) and the filtering mechanism (through the filter function) depend on the prescribed filtering level and are not fine-tuned based on the solution. In the original SCALES approach, due to the use of the nonlinear multi-resolution WTF, both the numerical grid and the filter width are constantly adapted on the solution. The threshold level of WTF for the numerical solver can coincide with or differ from the one used for turbulence modelling (De Stefano & Vasilyev 2013). However, similarly to the classical explicit LES, the wavelet threshold level is *a priori* defined, which results in the explicit prescription of the SGS kinetic energy level. This limitation is removed by the current fully-adaptive wavelet-thresholding formulation. The new *m*-SCALES method is based on a more objective user-defined physical measure that is, for instance, the FSGSD variable. The

WTF threshold is automatically and continuously adapted in order to maintain the desired level of resolution or fidelity.

For the sake of completeness, it should be mentioned that the spatially varying thresholding methodology is neither limited to SCALES nor exclusively designed for homogeneous flows. For instance, the forcing technique with characteristics-based tracking of ϵ has been tested for inhomogeneous flows at low Reynolds number by Nejadmalayeri (2012). The results for incompressible flow around complex geometry obstacles have demonstrated the robustness of the adaptation strategy. In the absence of SGS modelling, the forcing scheme can be defined, for example, in terms of the vorticity or rate-of-strain magnitude. The extension of the present methodology to CVS and WDNS of inhomogeneous turbulent flows at high Reynolds numbers is currently under investigation.

6. Numerical experiments

To demonstrate the functionality of the developed hybrid variable-fidelity methodology, two important measures are scrutinized: the accuracy of preserving the fraction of modelled dissipation $\mathcal{F}$, at the prescribed value $\mathcal{G}$, and the time response of the procedure to adjust to a change of the goal. The former measure indicates how accurately the method can really maintain the desired fidelity, while the latter shows how fast the overall turbulence resolution can be dynamically adjusted. Hence, the variable thresholding method should be thoroughly tested with the desired level of the physical quantity to be controlled constantly changing in space/time. In this section, the extreme case, namely the instantaneous change of the goal value $\mathcal{G}$, that corresponds to rapid switching between different regimes, is examined. If the methodology can deal with such abrupt changes, it surely can deal with continuous spatial changes.

The present numerical experiments are conducted for linearly forced homogeneous turbulence, according to the SCALES approach discussed in § 4. The forcing coefficient on the right-hand side of the filtered momentum equation (4.2) is set to $Q = 20/3$. Homogeneous turbulence simulation is a good test for the proposed methodology, since the resolved dissipation is highly intermittent in both space and time, thus requiring rapid spatio-temporal adjustment of wavelet threshold to maintain both local and volume-averaged turbulence resolutions at the required level. If the method is capable of retaining the desired turbulence resolution over many eddy turnover times (τ_{eddy}), or adjusting to a new goal within one τ_{eddy}, then the robustness of the proposed methodology is confirmed. It is worth noting that the FSGSD variable is controlled locally in space and, moreover, the method can also be applied with spatially varying prescribed resolution. For this reason, the proposed methodology would be fully applicable to inhomogeneous turbulent flows.

Both the approaches discussed in § 5 are used for the present experiments. The evolution equation (EE) method consists of solving the Lagrangian path-line diffusive averaging equation (5.1) together with the SCALES governing equations. The interpolation approach, which is based on (5.2), exploits either first- or third-order interpolation. In the EE approach, the additional artificial diffusion can be directly controlled through the coefficient C_{ν_ϵ} while, for the interpolation case, the first-order method is expected to introduce larger numerical diffusion compared to the third-order one.

To analyse both the accuracy of preserving the FSGSD and the time-response characteristics, a relatively complicated test case is constructed. It can be considered

as a simplified model of physical situations where the desired level of turbulence resolution is repeatedly altered every few τ_{eddy}. The simulation of linearly forced homogeneous turbulence at Taylor microscale Reynolds number $Re_\lambda \cong 70$ with non-adaptive effective 256^3 resolution is performed. The turbulent velocity field is initialized by a well-developed SCALES solution with constant thresholding (De Stefano & Vasilyev 2010). The following sequence of six goal values {0.2, 0.25, 0.3, 0.2, 0.3, 0.25} is assumed, while changing $\mathcal{G}$ every $5\tau_{eddy}$. The simulations were performed for both first- and third-order interpolation, as well as for the EE method with different diffusion coefficients, which are $C_{\nu_\epsilon} = 0.05$, 0.1, 0.5, 1, 4 and 5. As discussed in § 5, the condition $C_{\nu_\epsilon} < 1$ ensures diffusion time scale larger than convective time scale, i.e. convective-dominated transport. However, the greater values of C_{ν_ϵ} are intentionally selected so that this fact can be empirically proved. To prevent any unrealistic filtering, the threshold ϵ was bounded to $0.2 \leqslant \epsilon \leqslant 0.5$.

In this context, the turbulence resolution is measured by the total FSGSD, which is defined as $\overline{\mathcal{F}} = \langle \Pi \rangle / (\langle \varepsilon_{res} \rangle + \langle \Pi \rangle)$, where $\langle \Pi \rangle = \langle -\tau_{ij}^* \overline{S}_{ij}^{>\epsilon} \rangle$ and $\langle \varepsilon_{res} \rangle = 2\nu \langle \overline{S}_{ij}^{>\epsilon} \overline{S}_{ij}^{>\epsilon} \rangle$ are the volume-averaged modelled SGS and resolved viscous dissipation, respectively. The total FSGSD is reported for the interpolation and EE approaches in figures 3(*a*) and 3(*b*), respectively. In the former case, there is a time-response delay, which is by and large greater than one τ_{eddy}, resulting in slow adjustment to the newly prescribed goal value. This undesired and unrealistic response lag is not affected by the interpolation order. As the use of smaller diffusion coefficients in the EE approach can prevent this behaviour, it is concluded that the diffusion of the scheme causes the time-response delay.

In terms of the achieved turbulence resolution, it is observed that lower diffusion results in a total FSGSD $\overline{\mathcal{F}}$ that is closer to $\mathcal{G}$ during each time interval. The presence of large diffusion can significantly delay the time response of the solution, while affecting the level of accuracy of turbulence resolution. However, this diffusion is necessary since the threshold field must be maintained sufficiently smooth by preventing the formation of localized structures with sharp interfaces. In fact, the turbulent velocity is filtered using spatially varying thresholding and any noise in the threshold field can lead to significant noise and undesired small-scale fluctuations in the SCALES solution. Although with $C_{\nu_\epsilon} = 0.1$, no evidence of such instabilities is observed, a qualitative investigation of the threshold field smoothness is highly recommended. To demonstrate the effect of the numerical diffusion on the response characteristics of the method, the contour plots of threshold throughout the computational domain, for different values of C_{ν_ϵ} in the EE case, as well as for both first- and third-order interpolation, are examined in figure 4. The snapshots at two different time instants, which correspond to the beginning of the fourth interval ($t = 16\tau_{eddy}$) and the end of the sixth interval ($t = 29\tau_{eddy}$) are reported in figures 4(*a*) and 4(*b*), respectively.

By examining the time history of the global variable $\overline{\mathcal{F}}$, it is evident that the best response is achieved for $C_{\nu_\epsilon} = 0.1$. However, if the volume-averaged FSGSD $\langle \mathcal{F} \rangle = \langle \Pi / (\varepsilon_{res} + \Pi) \rangle$ is used for global monitoring, a better response is achieved for $C_{\nu_\epsilon} = 1$, while the faster adjustment still occurs for $C_{\nu_\epsilon} = 0.1$, as illustrated in figure 3(*c*). Therefore, selecting the most appropriate diffusion is a subjective choice, which depends on the global monitoring variable that is adopted. The difference between $\overline{\mathcal{F}}$ and $\langle \mathcal{F} \rangle$ is confirmed by another similar benchmark at the higher Taylor microscale Reynolds number of $Re_\lambda \cong 120$. Simulations with non-adaptive effective 512^3 numerical resolution, based on the sequence of goal values {0.35, 0.4, 0.45, 0.35, 0.45, 0.4}, are performed using the EE method with

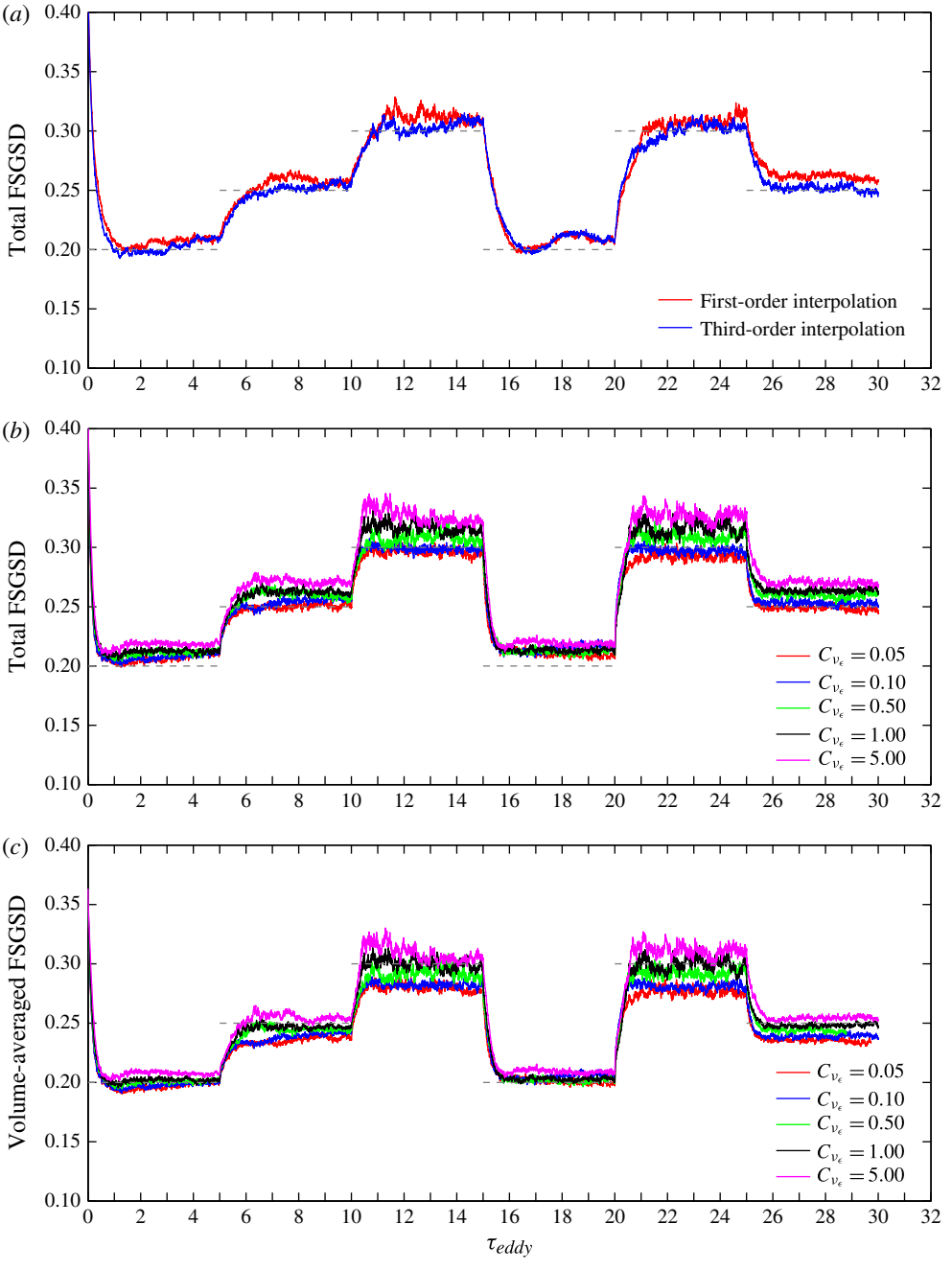

FIGURE 3. Time histories of total and volume-averaged FSGSD for m-SCALES with variable $\mathcal{G}$, using interpolation (first- and third-order) and EE method with different diffusion coefficients, at $Re_\lambda = 70$ with 256^3 numerical resolution. (a) Total FSGSD $\overline{\mathcal{F}} = \langle \Pi \rangle / (\langle \varepsilon_{res} \rangle + \langle \Pi \rangle)$ for interpolation method. (b) Total FSGSD $\overline{\mathcal{F}} = \langle \Pi \rangle / (\langle \varepsilon_{res} \rangle + \langle \Pi \rangle)$ for EE method. (c) Volume-averaged FSGSD $\langle \mathcal{F} \rangle = \langle \Pi / (\varepsilon_{res} + \Pi) \rangle$ for EE method.

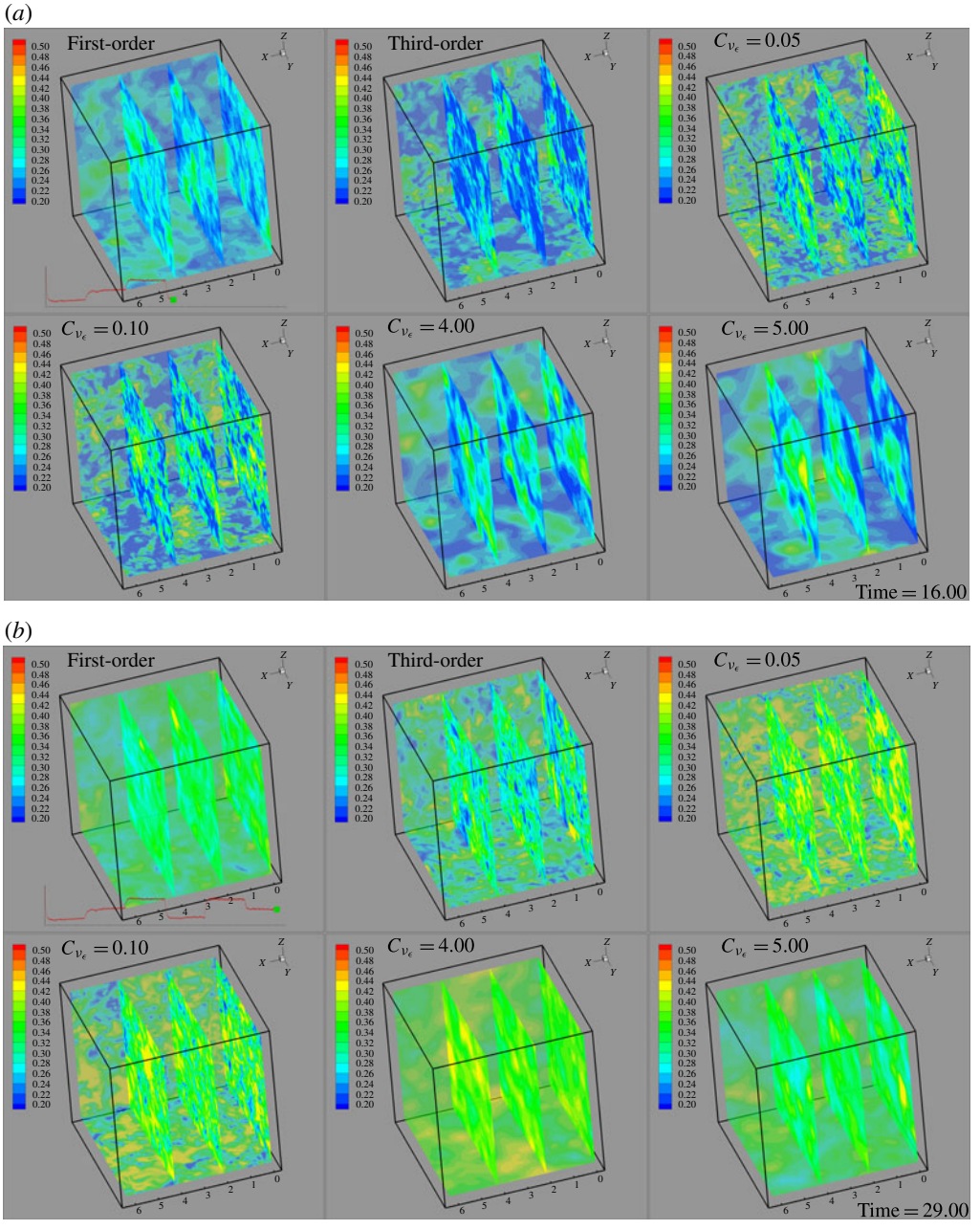

FIGURE 4. Threshold field contours at two different time instants for *m*-SCALES with variable $\mathcal{G}$, using interpolation (first- and third-order) and EE method with different diffusion coefficients, at $Re_\lambda = 70$ with 256^3 numerical resolution. (*a*) At the beginning of the fourth interval ($t = 16\tau_{eddy}$); (*b*) at the end of the sixth interval ($t = 29\tau_{eddy}$).

$C_{\nu_\epsilon} = 1$. The time histories illustrated in figure 5 show that the difference of these two measures is independent of Reynolds number. Indeed, the similar trends for both first- and third-order characteristic interpolation methods and the EE approach

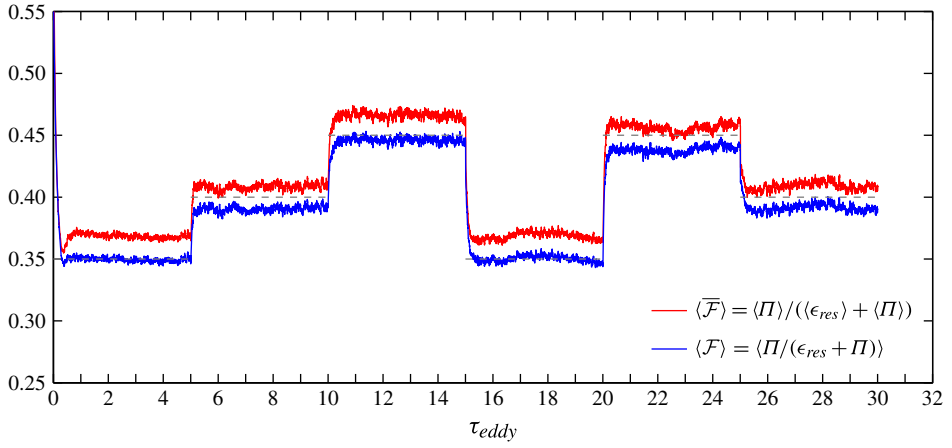

FIGURE 5. Time histories of total and volume-averaged FSGSD for *m*-SCALES with variable $\mathcal{G}$ using EE method with $C_{\nu_\epsilon} = 1$, at $Re_\lambda \cong 120$ with 512^3 numerical resolution.

with large diffusion coefficient using a sixth-order non-diffusive wavelet-based solver demonstrate the dominant role of the diffusion in controlling the transition between different fidelity regimes.

The time-averaged energy spectra for the EE case with $C_{\nu_\epsilon} = 0.1$ are shown in figure 6(*a*), for each of the six time periods during which $\mathcal{G}$ is kept constant. About two eddy turnover times are required for the transition from an achieved state to the next one. As expected, the representation of small scales improves by decreasing the goal $\mathcal{G}$, which confirms that the FSGSD variable $\mathcal{F}$ is a physically meaningful measure for the turbulence resolution. The prescribed goal actually takes only three different values, each repeated twice. The energy spectra for each pair of intervals corresponding to the same goal would be expected to coincide. This is not observed for the first ($2\tau_{eddy} < t < 4.8\tau_{eddy}$) and fourth ($17\tau_{eddy} < t < 19.8\tau_{eddy}$) intervals, which correspond to $\mathcal{G} = 0.2$. During the first time interval, since $\mathcal{G}$ has the smallest value, the solution should be expected to show the highest energy spectra whereas, at small wavenumbers, these spectra show the lowest energy. In fact, the velocity field is initialized by a SCALES solution with constant high threshold, corresponding to a large value of FSGSD, and is forced to converge to a relatively high level of resolution. Apparently, the converged state is actually not achieved. On the contrary, during the fourth interval, given the different starting conditions, a more realistic energy spectrum is observed.

The time-averaged dissipation spectra are illustrated in figure 6(*b*), for the same case and six time intervals of figure 6(*a*). An important point to clarify is the presence of a jump in both energy and dissipation spectra at a wavenumber of $\kappa = 64$. In fact, the effective resolution is not always the maximum available, which corresponds to 256^3 grid points, but occasionally falls to 128^3. This peculiar feature of the adaptive wavelet-based methods is clearly illustrated in figure 7, where the scatter plots of the retained wavelet collocation points, coloured by the level of resolution, are reported for CVS and SCALES. The two different calculations are performed starting from the same initial conditions, with the same 256^3 numerical resolution. For the CVS solution, which matches the WDNS up to the dissipation range, the wavelet collocation grid is adapted to the highest level of resolution ($j = 6$) at few locations.

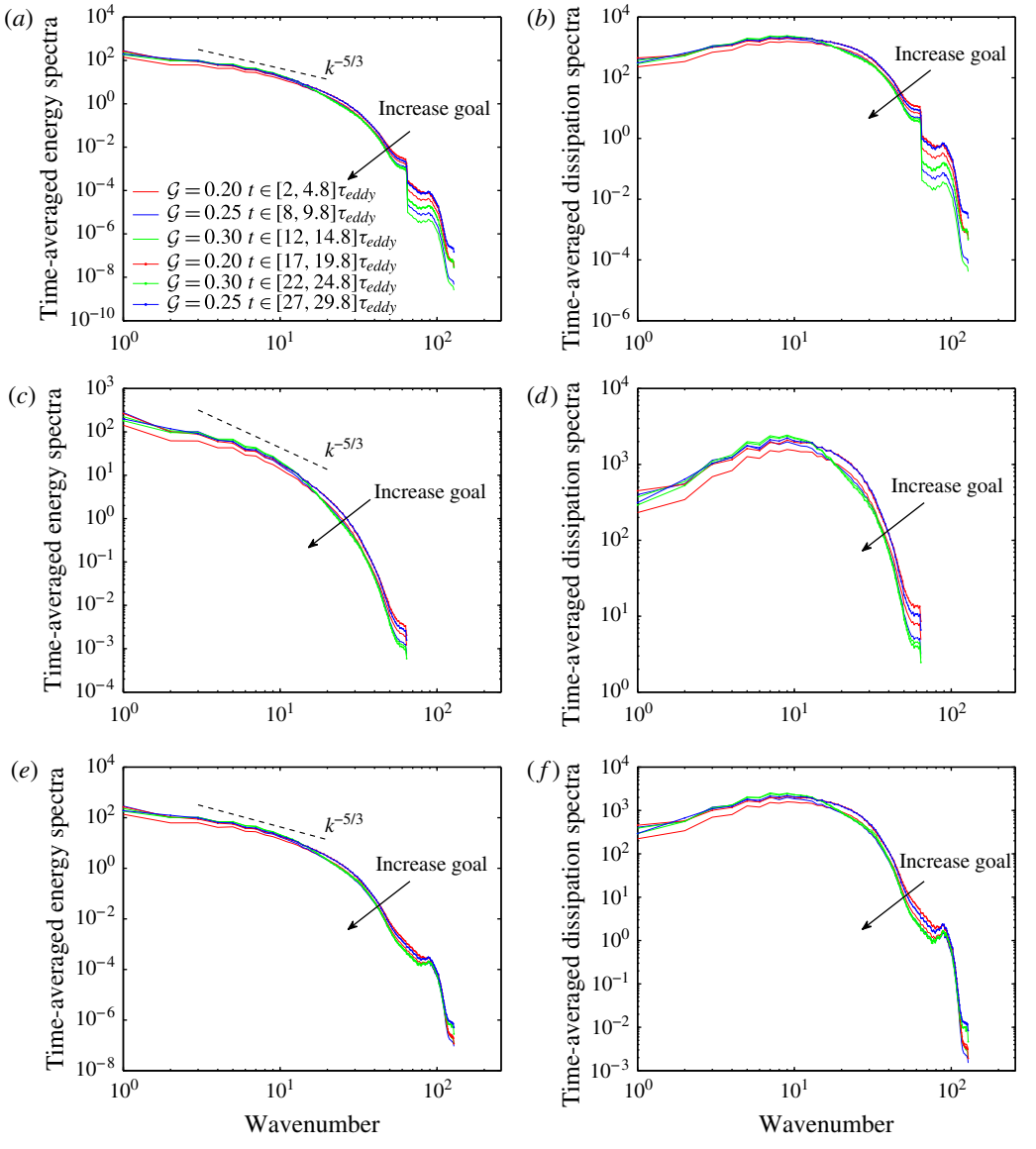

FIGURE 6. Time-averaged energy and dissipation spectra for m-SCALES with variable $\mathcal{G}$, corresponding to EE method with $C_{\nu_\epsilon} = 0.1$, at $Re_\lambda = 70$ with 256^3 numerical resolution. (a,b) For all κ; (c,d) $\kappa_{max} = 64$; (e,f) $\kappa_{max} = 128$.

For SCALES, which matches the CVS up to the inertial range, the highest level of resolution almost always corresponds to $j = 5$. Due to the action of SGS modelling, effective coarser resolution is more probable in SCALES, where the 256^3 resolution is rarely involved. Thus, SCALES can resolve the most energetic turbulent structures, which are responsible for the energy cascade, not only by using adaptive resolution but even with a smaller maximum resolved wavenumber. Therefore, the kink in the time-averaged spectra appears because the maximum actual resolution is just 128^3 at various time instants, as a result of time-averaging spectra with different maximum

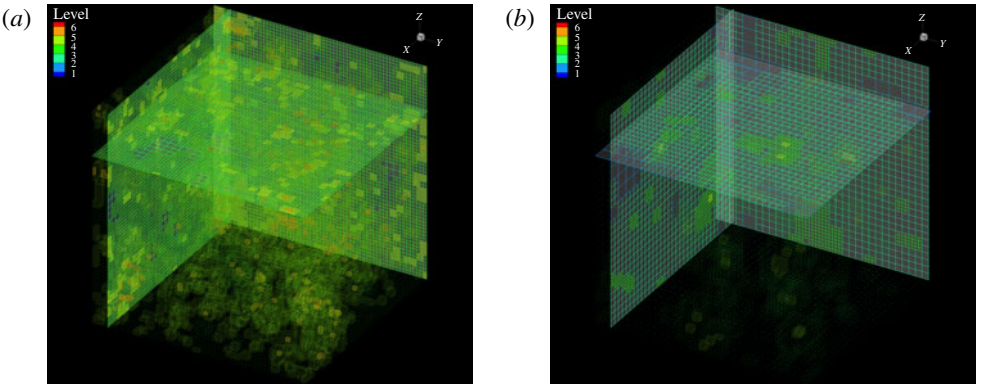

FIGURE 7. Scatter plot of the retained wavelet collocation points, coloured by the level of resolution $1 \leqslant j \leqslant 6$, for (*a*) CVS and (*b*) SCALES with 256^3 numerical resolution.

wavenumbers of 64 and 128. This is confirmed by inspection of figures 6(*c–f*), where the energy and dissipation spectra obtained by averaging the time frames with only either $\kappa_{max} = 64$ or $\kappa_{max} = 128$ are shown.

To further analyse the proposed approach, while fully justifying that the FSGSD parameter $\mathcal{F}$ represents a physically meaningful measure of the turbulence resolution, a series of simulations with different constant goal values are performed. As for homogeneous turbulence the resolved dissipation is highly intermittent, the main objective is to ensure that the total FSGSD $\overline{\mathcal{F}}$ remains approximately constant for each prescribed turbulence resolution. Also, since an increase of $\mathcal{G}$ implies that fewer turbulent eddies are resolved, the modelled SGS dissipation should increase with this parameter. In order to study how the fidelity of the simulation influences these two characteristics, several simulations are carried out for different fidelity turbulence resolutions, on adaptive grids with maximum 256^3, 512^3, and 1024^3 numerical resolutions. These computations are conducted by keeping constant the ratio of Kolmogorov dissipation length scale to the smallest grid spacing, i.e. $\eta/\Delta_{min} \cong 2$, so that the maximum available numerical resolution is maintained adequate for a well-resolved WDNS. By doubling the effective resolution the viscosity must be decreased by a factor of $2^{4/3}$. In fact, denoting as $\mathrm{I}\!\Omega_{1D}$ the non-adaptive effective resolution in each direction, $\Delta_{min} \sim \mathrm{I}\!\Omega_{1D}^{-1}$. Since $\Delta_{min} \sim \eta$ and $\eta \sim \nu^{3/4}$, as a consequence, $\nu \sim \mathrm{I}\!\Omega_{1D}^{-4/3}$. The three different viscosity coefficients used in the simulations are $\nu = 0.09$, 0.035 and 0.015. Owing to the Taylor microscale Reynolds number definition, that corresponds to having linearly forced homogeneous turbulence solutions at $Re_\lambda \cong 70$, 120 and 190, respectively.

The different fidelity is achieved by using the spatially varying thresholding approach with different goal values, namely $\mathcal{G} = 0.2$, 0.25, 0.32, 0.4 and 0.5. The total dissipation ratio $\overline{\mathcal{F}}$ actually remains nearly the same for each level of turbulence resolution, as illustrated in figure 8, where the time histories of this parameter are reported for the different experiments. Thus, the methodology is capable of preserving a constant level of turbulence resolution over many eddy turnover times, regardless of the Reynolds number. Moreover, as expected, by increasing the goal $\mathcal{G}$, turbulence is less resolved and, as a result, the volume-averaged SGS dissipation $\langle \Pi \rangle$ increases, as illustrated in figure 9. This comprehensive Reynolds-number independency study demonstrates that the developed hybrid adaptive variable-fidelity multi-resolution

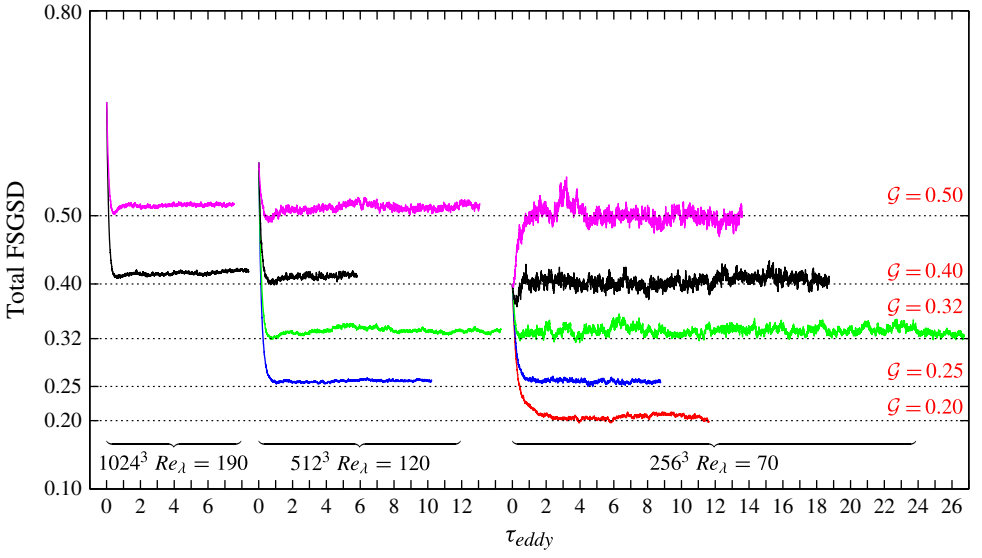

FIGURE 8. Time history of total FSGSD $\overline{\mathcal{F}}$ for *m*-SCALES with constant goal, at various levels of turbulence resolution.

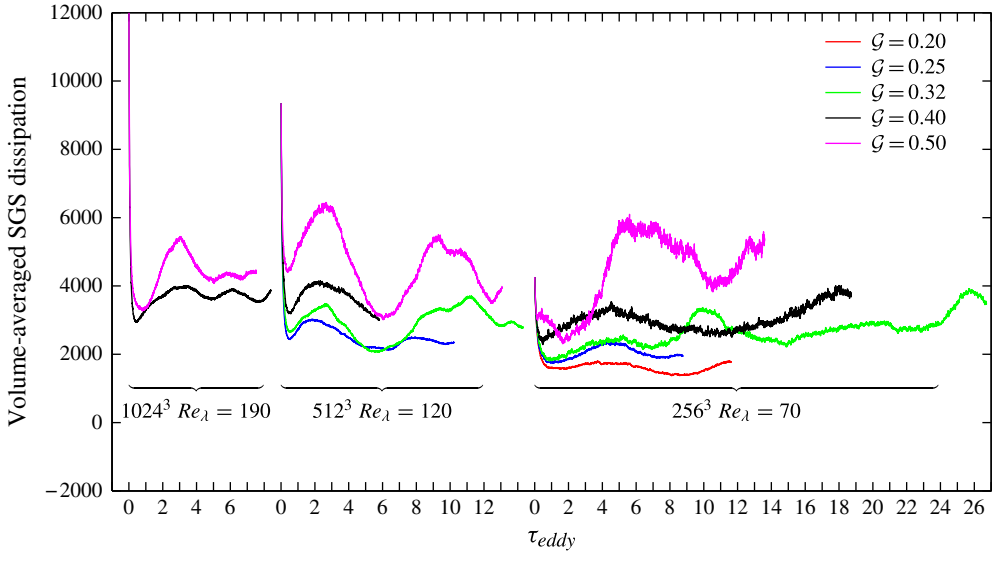

FIGURE 9. Time history of volume-averaged SGS dissipation $\langle \Pi \rangle$ for *m*-SCALES with constant goal, at various levels of turbulence resolution.

methodology can be successfully applied at any Reynolds number, by also confirming that the FSGSD variable (5.3) stands for a physically meaningful quantity that measures the fidelity of the solution, regardless of the Reynolds number.

The computational efficiency of the present method can be evaluated by considering the number of active wavelets (say $\mathfrak{N}$), since the computational cost for the PAWCM

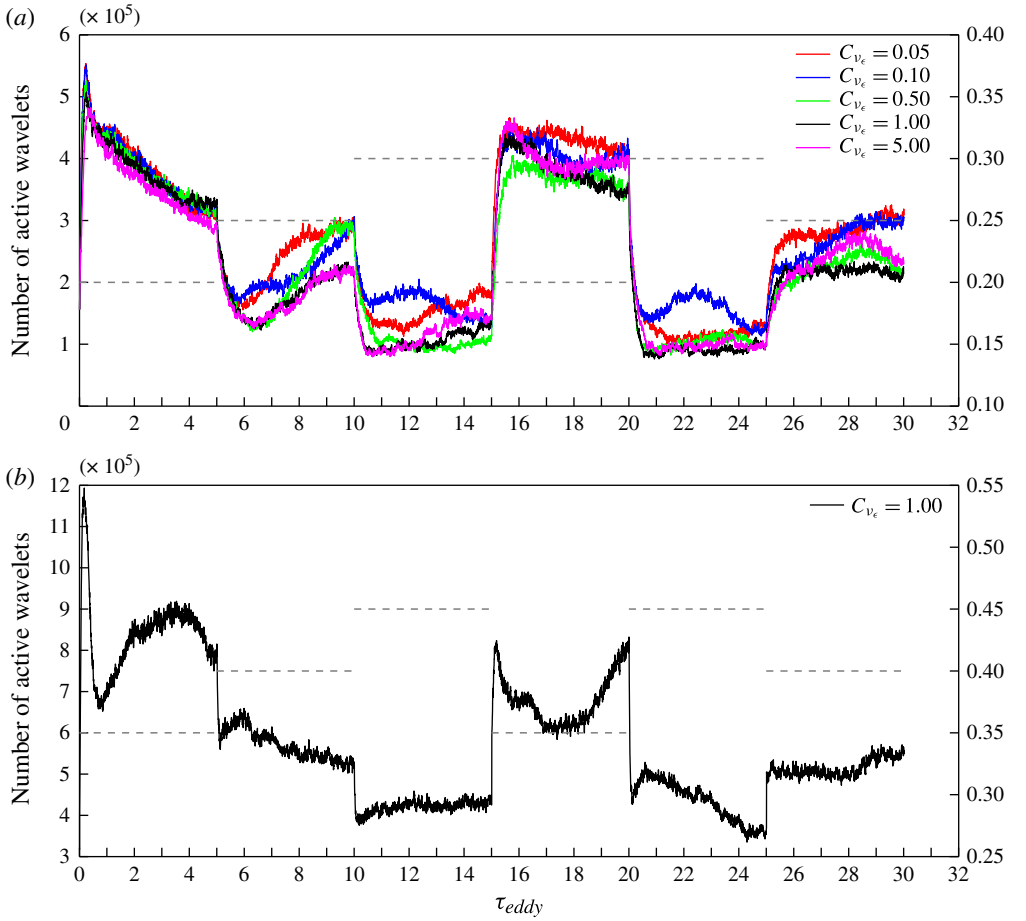

FIGURE 10. Number of active wavelets and corresponding goal levels of turbulence resolution for m-SCALES using the EE method with various diffusion coefficients, at two different Reynolds numbers. Horizontal dashed lines and the corresponding right-hand axis indicate the values of $\mathcal{G}$. (*a*) 256^3, $Re_\lambda = 70$. (*b*) 512^3, $Re_\lambda = 120$.

technique is of $O(\mathfrak{I})$. In figure 10, the time histories of $\mathfrak{I}$ for SCALES solutions with variable goal are depicted. The computations are performed at $Re_\lambda \cong 70$ and 120, corresponding to the same cases as figures 3 and 5, respectively. The computational cost significantly increases as $\mathcal{G}$ decreases, and vice versa. For instance, the number $\mathfrak{I}_{\mathcal{G}=0.2}$ is nearly twice $\mathfrak{I}_{\mathcal{G}=0.25}$. The same behaviour is observed for SCALES experiments where $\mathcal{G}$ is kept constant in time, which are illustrated in figure 11, corresponding to the same cases as figures 8 and 9. It is worth noting that the change in computational cost with $\mathcal{G}$ is slightly amplified with increasing Reynolds number. For instance, by increasing the goal from 0.4 to 0.5, the ratio of $\mathfrak{I}_{\mathcal{G}=0.4}/\mathfrak{I}_{\mathcal{G}=0.5}$ is approximately 1.5, 1.8, and 2.1 at $Re_\lambda = 70$, 120 and 190, respectively.

The grid compression can be measured by the ratio $\mathfrak{I}/\mathfrak{I}_{max}$, where $\mathfrak{I}_{max}$ is the total number of wavelets available on the non-adaptive effective grid at the highest level of resolution. For instance, given the goal $\mathcal{G} = 0.4$, $\mathfrak{I}/\mathfrak{I}_{max}$ drops from 0.45 % to 0.35 % when Re_λ increases from 120 to 190. This makes the SCALES approach

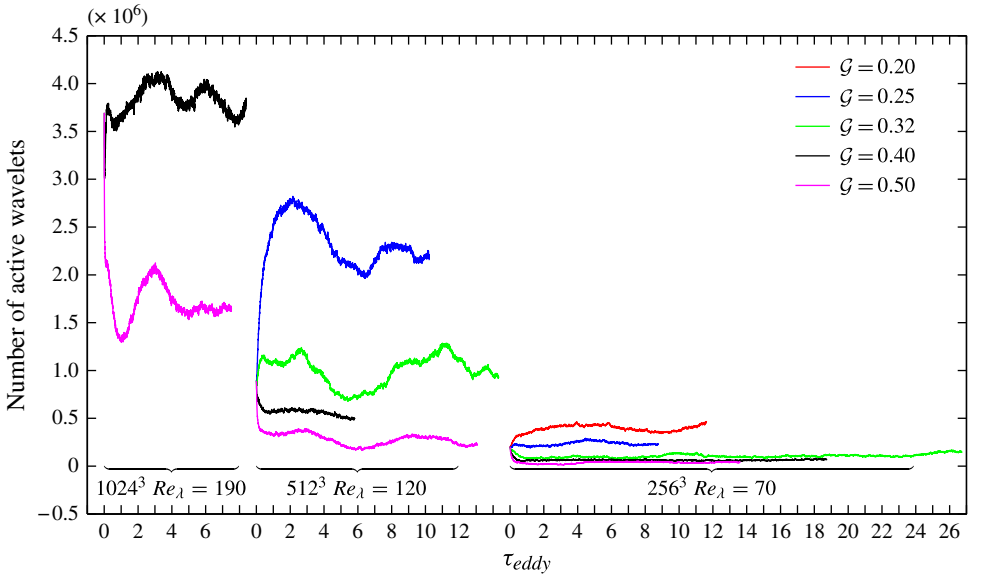

FIGURE 11. Number of active wavelets for *m*-SCALES with constant goal, corresponding to various levels of turbulence resolution, at three different Reynolds numbers.

even more efficient for high-Reynolds-number flows. Considering that the sixth-order PAWCM solver is approximately three- to five-times slower per grid point than a pseudo-spectral DNS solver (De Stefano & Vasilyev 2010), even using 2 % of the available wavelets (at the worst case scenario) would provide an acceleration of approximately 16–10 times with respect to pseudo-spectral DNS. This clarifies why the high-compression property is the main strength of wavelet-based methods for turbulence modelling.

As already pointed out when discussing the spectra depicted in figure 6, the turbulence resolution degrades with the resolved fraction of dissipation, that is, by increasing the prescribed goal for the variable $\mathcal{F}$. The quality of the different numerical solutions is further examined by considering high-order statistics. In figure 12, both the skewness and kurtosis of velocity, velocity-derivative and second-velocity-derivative are illustrated for SCALES with variable goal, corresponding to the EE method with two different diffusion coefficients, at $Re_\lambda = 70$. Also, the velocity-derivative skewness for SCALES with constant goal at various turbulent resolutions is considered in figures 13(*a*) and 13(*b*), at $Re_\lambda = 70$ and 120, respectively. It is observed, in particular, that smaller values of skewness correspond to smaller values of $\mathcal{G}$.

The present experiments have demonstrated the proposed methodology as a very robust single framework for performing fully adaptive turbulence simulations. The fact that the volume-average of the localized FSGSD variable, which is very rapidly and randomly varying in space and time for homogeneous turbulence, could be maintained approximately constant and altered quickly, demonstrates how efficient the proposed approach is. Furthermore, the method is expected to be even more efficient for inhomogeneous flow applications, where the spatial/temporal variations of the FSGSD are expected to be smooth.

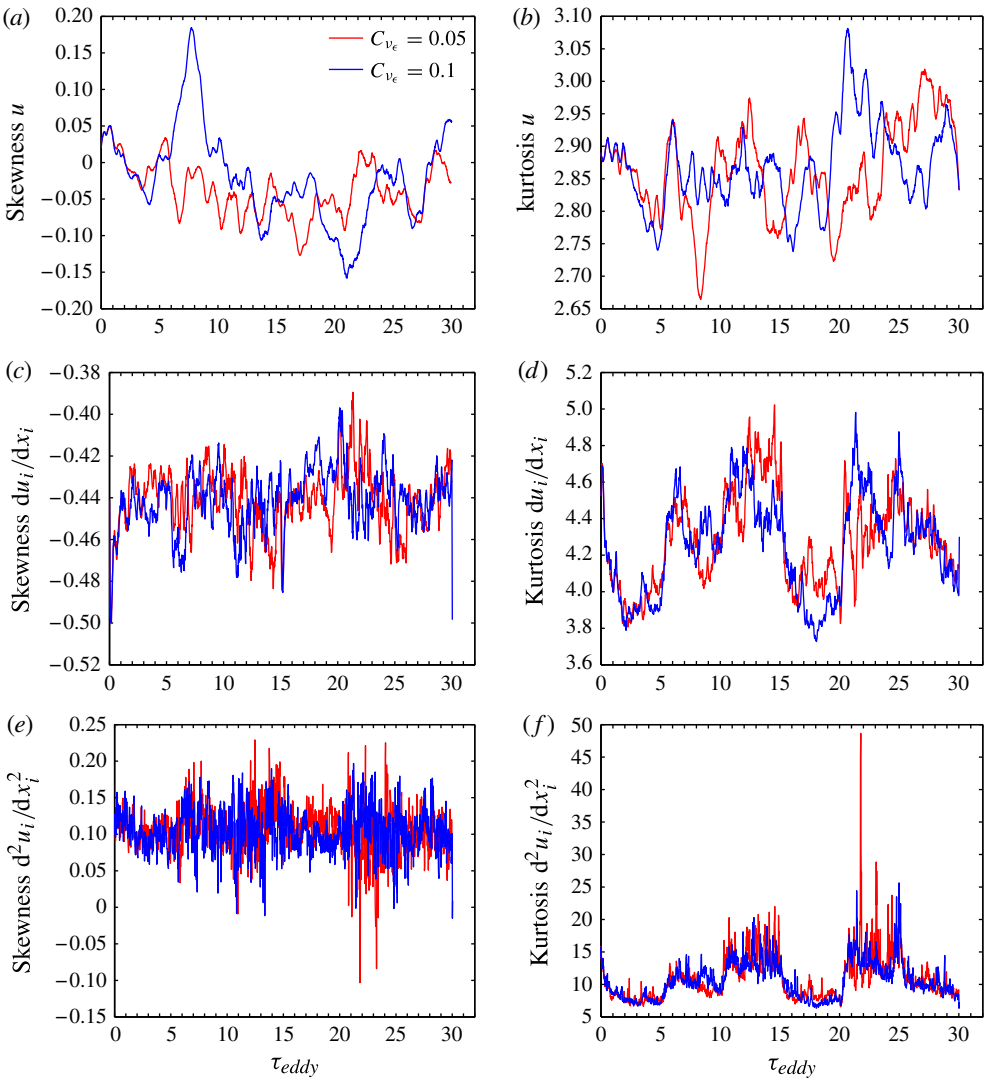

FIGURE 12. Skewness and kurtosis of (*a,b*) velocity, (*c,d*) velocity-derivative and (*e,f*) second-velocity-derivative for SCALES with variable goal, corresponding to EE method with $C_{\nu_\epsilon} = 0.05$ and 0.1, at $Re_\lambda = 70$ with 256^3 numerical resolution.

7. Conclusions

This work represents the first successful attempt to develop a hybrid wavelet-based adaptive approach to turbulence modelling. The method is based on a wavelet thresholding filter (WTF) with spatio-temporally varying threshold and exploits the Lagrangian representation of the variable threshold. The proposed methodology can be referred to as *hierarchical multi-scale adaptive variable-fidelity wavelet-based turbulence modelling*. It represents a very robust framework for performing hybrid turbulence simulations, analogous to the hybrid non-adaptive RANS/LES/DNS approach. Within this framework, only one numerical solver is utilized and the challenges corresponding to overlapping multiple solvers and using Adaptive Mesh Refinement (AMR) procedures are irrelevant.

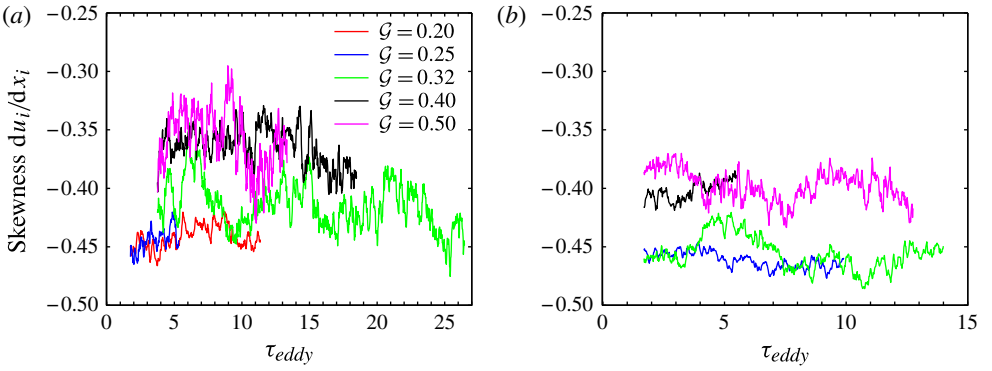

FIGURE 13. Skewness of velocity-derivative for SCALES with constant goal, corresponding to various levels of turbulence resolution, at two different Reynolds numbers: (*a*) $Re_\lambda = 70,\ 256^3$; (*b*) $Re_\lambda = 120,\ 512^3$.

The methodology provides the automatic two-way transition between different wavelet-based computational approaches. WDNS, where all significant flow structures are resolved, CVS, where coherent/incoherent flow decomposition is exploited, and SCALES, where the energy-containing motions are resolved while modelling the effect of less energetic coherent/incoherent eddies, are considered in a unique framework. This defines a new concept of turbulence model refinement, which is named *m*-refinement.

The numerical experiments presented in this work utilize a goal value for global turbulent resolution, which is either varying or constant in time. The more realistic case where the prescribed goal is spatially varying will be considered for future applications to inhomogeneous turbulent flows. The developed scheme, which is demonstrated to perfectly work in the homogeneous case, is expected to be even more effective for inhomogeneous turbulence, where more energetic organized flow structures exist.

Due to the enormous compression of wavelets, the developed hybrid method makes variable-fidelity turbulence simulations feasible on very large domains and at large Reynolds numbers. Finally, in order to make the proposed variable-fidelity approach more applicable to high-Reynolds-number engineering flows, it should be extended to lower-fidelity models such as the WURANS approach. However, in addition to changing/controlling the wavelet thresholding factor, the complete WDNS/CVS/SCALES/WURANS simulations require the development of new model form adaptation and coupling strategies specific to wavelet methods. This work is currently underway.

Acknowledgements

This work was supported by the National Science Foundation (NSF) under grant nos CBET-0756046 and CBET-1236505. This support is gratefully acknowledged. Authors are also thankful for the computing time on the Janus supercomputer, which is supported by the NSF (award number CNS-0821794) and the University of Colorado Boulder. The Janus supercomputer is a joint effort of the University of Colorado Boulder, the University of Colorado Denver and the National Centre for Atmospheric Research.

REFERENCES

CHAOUAT, B. & SCHIESTEL, R. 2005 A new partially integrated transport model for subgrid-scale stresses and dissipation rate for turbulent developing flows. *Phys. Fluids* **17** (6), 065106.1–065106.19; http://dx.doi.org/10.1063/1.1928607.

DAUBECHIES, I. 1992 *Ten Lectures on Wavelets*, CBMS-NSF Series in Applied Mathematics, vol. 61. SIAM.

DE STEFANO, G. & VASILYEV, O. V. 2010 Stochastic coherent adaptive large eddy simulation of forced isotropic turbulence. *J. Fluid Mech.* **646**, 453–470.

DE STEFANO, G. & VASILYEV, O. V. 2012 A fully adaptive wavelet-based approach to homogeneous turbulence simulation. *J. Fluid Mech.* **695**, 149–172.

DE STEFANO, G. & VASILYEV, O. V. 2013 Wavelet-based adaptive large-eddy simulation with explicit filtering. *J. Comput. Phys.* **238**, 240–254.

DE STEFANO, G., VASILYEV, O. V. & GOLDSTEIN, D. E. 2008 Localized dynamic kinetic-energy-based models for stochastic coherent adaptive large eddy simulation. *Phys. Fluids* **20**, 045102.

FARGE, M. & RABREAU, G. 1988 Transformee en ondelettes pour detecter et analyser les structures coherentes dans les ecoulements turbulents bidimensionnels. *C. R. Acad. Sci. Paris* II **307**, 1479–1486.

FARGE, M. & SCHNEIDER, K. 2001 Coherent vortex simulation (CVS), a semi-deterministic turbulence model using wavelets. *Flow Turbul. Combust.* **6**, 393–426.

FARGE, M., SCHNEIDER, K. & KEVLAHAN, N. K.-R. 1999 Non-Gaussianity and coherent vortex simulation for two-dimensional turbulence using an adaptive orthogonal wavelet basis. *Phys. Fluids* **11** (8), 2187–2201.

FRÖHLICH, J. & SCHNEIDER, K. 1996 Numerical simulation of decaying turbulence in an adaptive wavelet basis. *Appl. Comput. Harmon. Anal.* **3**, 393–397.

GHOSAL, S., LUND, T. S., MOIN, P. & AKSELVOLL, K. 1995 A dynamic localization model for large-eddy simulation of turbulent flows. *J. Fluid Mech.* **286**, 229–255.

GIRIMAJI, S. S. & WALLIN, S. 2013 Closure modelling in bridging regions of variable-resolution (VR) turbulence computations. *J. Turbul.* **14** (1), 72–98.

GOLDSTEIN, D. E. & VASILYEV, O. V. 2004 Stochastic coherent adaptive large eddy simulation method. *Phys. Fluids* **16** (7), 2497–2513.

GOLDSTEIN, D. E., VASILYEV, O. V. & KEVLAHAN, N. K.-R. 2005 CVS and SCALES simulation of 3D isotropic turbulence. *J. Turbul.* **6** (37), 1–20.

JAMESON, L. 1998 A wavelet-optimized, very high order adaptive grid and order numerical method. *SIAM J. Sci. Comput.* **19** (6), 1980–2013.

KEVLAHAN, N. K.-R., ALAM, J. M. & VASILYEV, O. V. 2007 Scaling of space–time modes with Reynolds number in two-dimensional turbulence. *J. Fluid Mech.* **570**, 217–226.

LIU, Q. & VASILYEV, O. V. 2006 Hybrid adaptive wavelet collocation-brinkman penalization method for DNS and URANS simulations of compressible flow around bluff bodies. *AIAA Paper* 2006-3206.

LUNDGREN, T. S. 2003 Linearly forced isotropic turbulence. *Annu. Res. Briefs*, pp. 461–473. Center for Turbulence Research, Stanford University.

MENEVEAU, C., LUND, T. S. & CABOT, W. H. 1996 A Lagrangian dynamic subgrid-scale model of turbulence. *J. Fluid Mech.* **319**, 353–385.

NEJADMALAYERI, A. 2012 Hierarchical multiscale adaptive variable fidelity wavelet-based turbulence modelling with Lagrangian spatially variable thresholding. PhD thesis, University of Colorado Boulder, Boulder, CO.

NEJADMALAYERI, A., VASILYEV, O. V., VEZOLAINEN, A. & DE STEFANO, G. 2011 Spatially variable thresholding for stochastic coherent adaptive LES. In *Proceedings of Direct and Large-Eddy Simulation Workshop 8: Eindhoven University of Technology, the Netherlands, July 7–9, 2010* (ed. H. Kuerten, B. Geurts, V. Armenio & J. Fröhlich), pp. 95–100. Springer.

ROSALES, C. & MENEVEAU, C. 2005 Linear forcing in numerical simulations of isotropic turbulence: physical space implementations and convergence properties. *Phys. Fluids* **17**, 1–8.

SCHIESTEL, R. & DEJOAN, A. 2005 Towards a new partially integrated transport model for coarse grid and unsteady turbulent flow simulations. *Theor. Comput. Fluid Dyn.* **18** (6), 443–468.

SCHNEIDER, K. & VASILYEV, O. V. 2010 Wavelet methods in computational fluid dynamics. *Annu. Rev. Fluid Mech.* **42**, 473–503.

SWELDENS, W. 1996 The lifting scheme: a custom-design construction of biorthogonal wavelets. *Appl. Comput. Harmon. Anal.* **3** (2), 186–200.

VASILYEV, O. V., DE STEFANO, G., GOLDSTEIN, D. E. & KEVLAHAN, N. K.-R. 2008 Lagrangian dynamic SGS model for SCALES of isotropic turbulence. *J. Turbul.* **9** (11), 1–14.